

# Constraining the low-mass end of the Initial Mass Function with Gravitational Lensing

Ignacio Ferreras<sup>1\*</sup>, Prasenjit Saha<sup>2</sup>, Dominik Leier<sup>3</sup>,  
Frédéric Courbin<sup>4</sup> and Emilio E. Falco<sup>5</sup>

<sup>1</sup> Mullard Space Science Laboratory, University College London, Holmbury St Mary, Dorking, Surrey RH5 6NT

<sup>2</sup> Institute for Theoretical Physics, University of Zürich, Winterthurerstr. 190, CH-8057 Zürich, Switzerland

<sup>3</sup> Astronomisches Rechen-Institut, Zentrum für Astronomie, Universität Heidelberg, Mönchhofstr. 12-14, D-69120 Heidelberg, Germany

<sup>4</sup> Laboratoire d'astrophysique, École Polytechnique Fédérale de Lausanne (EPFL), Observatoire de Sauverny, 1290 Versoix, Switzerland

<sup>5</sup> Harvard-Smithsonian Center for Astrophysics, 60 Garden Street, Cambridge, MA 02138, USA

MNRAS Letters, Accepted 2010 August 24. Received 2010 August 23; in original form 2010 July 26

## ABSTRACT

The low-mass end of the stellar Initial Mass Function (IMF) is constrained by focusing on the baryon-dominated central regions of strong lensing galaxies. We study in this letter the Einstein Cross (Q2237+0305), a  $z=0.04$  barred galaxy whose bulge acts as lens on a background quasar. The positions of the four quasar images constrain the surface mass density on the lens plane, whereas the surface brightness (H-band NICMOS/HST imaging) along with deep spectroscopy of the lens (VLT/FORS1) allow us to constrain the stellar mass content, for a range of IMFs. We find that a classical single power law (Salpeter IMF) predicts more stellar mass than the observed lensing estimates. This result is confirmed at the 99% confidence level, and is robust to systematic effects due to the choice of population synthesis models, the presence of dust, or the complex disk/bulge population mix. Our non-parametric methodology is more robust than kinematic estimates, as we do not need to make any assumptions about the dynamical state of the galaxy or its decomposition into bulge and disk. Over a range of low-mass power law slopes (with Salpeter being  $\Gamma = +1.35$ ) we find that at a 90% confidence level, slopes with  $\Gamma > 0$  are ruled out.

**Key words:** galaxies: individual: 2237+0305 – galaxies: stellar content – stars: luminosity function, mass function – gravitational lensing.

## 1 INTRODUCTION

The stellar Initial Mass Function (IMF) is defined as the starting mass distribution of a stellar population. A large number of studies have targeted its shape and possible universality (see e.g. Kroupa 2002; Larson 2006; Kroupa 2007; Bastian et al. 2010). It has important implications in the formation and evolution of galaxies as it affects the chemical enrichment process and determines the stellar mass content of galaxies. The seminal work of Salpeter (1955) assumed a single power law distribution between the upper ( $\sim 100\text{--}120M_{\odot}$ ) and lower mass cutoffs ( $0.07M_{\odot}$ ). More recently, the “local IMF” has been constrained in more detail, with a turnover at lower masses (Andersen et al. 2008), and a characteristic mass around  $\sim 1M_{\odot}$  (Larson 1998).

Constraining the IMF outside our Galaxy is a challenging task. Data from unresolved stellar populations are very degenerate with respect to their properties such as age, metallicity or dust

content. Furthermore, changes in the low-mass end of the IMF do not translate into significant changes of the photo-spectroscopic observables, mainly because of the small contribution from low-mass stars to the net luminosity budget of a galaxy. However, changes in the low-mass end of the IMF result in measurable changes of the total stellar mass of a given population. Therefore, any attempt at constraining the low-mass end of the IMF requires an independent measure of the stellar mass content of the galaxy. Cappellari et al. (2006) compared the kinematic data from a number of SAURON early-type galaxies with dynamical models, and concluded that a single power law for the IMF (à la Salpeter) was ruled out. Using gravitational lensing in the inner, baryon-dominated, regions of early-type galaxies, Ferreras et al. (2008) showed that a Salpeter IMF produced too much stellar mass compared to the lensing mass within the same region. In this paper we extend the gravitational lensing analysis and the modelling work, to give a more quantitative constraint on the low-mass end of the IMF. We study in this letter a nearby strong lens, the Einstein Cross (Q2237+0305 Huchra et al. 1985), combining high resolution NIR imaging with

\* E-mail: ferreras@star.ucl.ac.uk

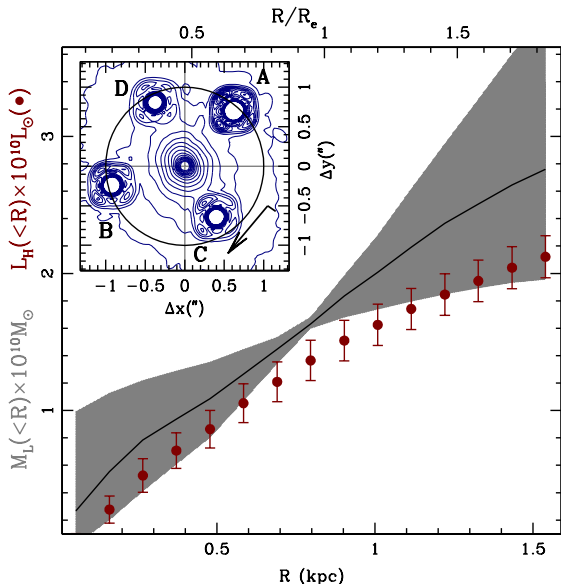


**Figure 1.** Cumulative lensing mass profile (shaded region) and luminosity (dots). 90% confidence levels shown. Notice the butterfly-shape of the uncertainty for lensing mass, which is minimal at the position on the lens plane of the images of the background source. The inset shows a contour map of the F160W HST/NICMOS image. At the lens position 1 arcsec maps into 0.77 kpc. The arrow points North, the small segment from the base of the arrow points East.

HST/NICMOS and a deep spectrum of the lensing galaxy taken with the VLT, using the FORS1 instrument, to constrain the properties of the stellar populations.

The reason for choosing this lens is the exceptionally low redshift ( $z=0.04$ ) of the lensing galaxy. This has two advantages. First, it helps increase the signal-to-noise. Second, and even more important, the low lens redshift makes a strong lens from the innermost and densest part of the galaxy. The mass-to-light ratio is close to unity in the lensing region (see Figures 1 and 2 below). In other words, the lens is dominated by stars, and hence particularly well-suited to constraining the IMF. In contrast, typical galaxy lenses contain a significant dark-matter contribution.

A different approach using lensing galaxies has been recently taken by Treu et al. (2010) and Auger et al. (2010). Rather than choosing a single lens with minimal dark matter and maximal signal-to-noise, they choose a large sample of lenses, and attempt to subtract off the dark matter by fitting dark-matter profiles based on simulations. Their results favour a Salpeter IMF. However, a caveat in the method (as noted by Treu et al. 2010) is that if the assumed dark-matter profile is slightly too shallow, the stellar mass will be systematically overestimated, and a “heavy” IMF derived. If this is in fact the case, that would explain the apparent contradiction with the Ferreras et al. (2008) result, which excludes a Salpeter IMF for a subset of the same galaxies.

## 2 CONSTRAINING THE IMF

In order to constrain the low-mass end of the IMF, we need to combine stellar population synthesis with an independent estimate of total mass in a system whose total mass content is preferably (but not necessarily) dominated by the stellar mass. We note that even though baryonic, non-stellar matter (e.g. gas and dust) will con-

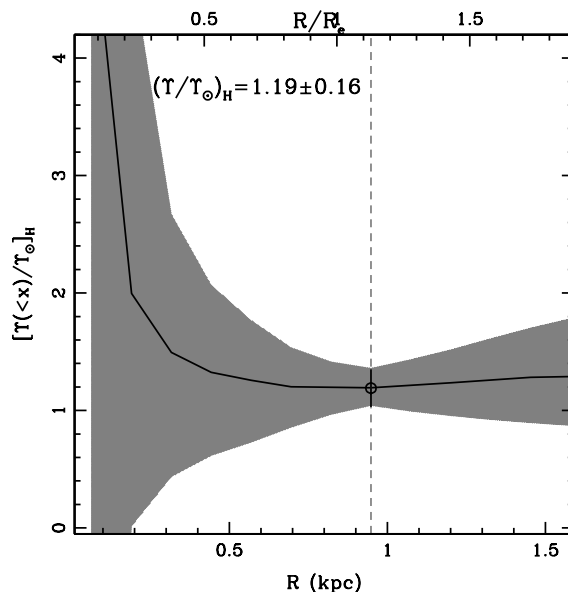


**Figure 2.** Predicted H-band mass to light ratio combining the analysis of the lensing data and the luminosity profile of the lens. The dot corresponds to the value chosen in this paper to constrain the stellar M/L, with mean and standard deviation as labelled.

tribute to the mass budget, the constraints on the IMF imposed in this letter go in the sense that rejected choices of the IMF predict *more* stellar mass than the total mass determined by the lens geometry. We use strong gravitational lensing as the independent estimator of mass. Kinematics-based methods have been used recently to quantify the total mass in the inner regions of galaxies (see e.g. Cappellari et al. 2006; Coccato et al. 2009). However, such methods rely on a particular definition of the dynamical system.

The lens is modelled using the *PixeLens* method (Saha & Williams 2004; Coles 2008), whereby the projected mass distribution is reconstructed as a pixellated mass map, which is not limited to any parametric form (cf. Trott et al. 2010) but can be any non-negative distribution subject to the following prior conditions. (i) The mass map is symmetric under a  $180^\circ$  rotation about the centre of brightness. (ii) The local density gradient must point no more than  $45^\circ$  away from the centre, which is assumed to coincide with the light peak. (iii) No pixel, except the central one, is allowed to be more than twice the mean of its neighbours. (iv) The circular average of the projected density, falls off as  $R^{-1/2}$  or steeper. In other words, the effective three-dimensional mass profile should be  $\propto r^{-3/2}$  or steeper.

The above requirements do not give a unique mass map, because solutions of the lens equation are highly non-unique (Falco et al. 1985; Saha 2000; Liesenborgs et al. 2008). Accordingly, the possible “model space” is sampled by an ensemble of 300 models. A useful property of the ensemble, due to the linear nature of the observational and prior constraints, is that the ensemble average is also a valid model; for comparisons of ensemble averages with individual models in *PixeLens*, see Figures 7 and 8 in Saha & Williams (2006).

For this study, we select the Einstein Cross (Huchra et al. 1985), where the bulge of a barred Sab galaxy at  $z=0.0394$  acts as a lens, generating a quadruple image of a background  $z=1.695$  QSO.

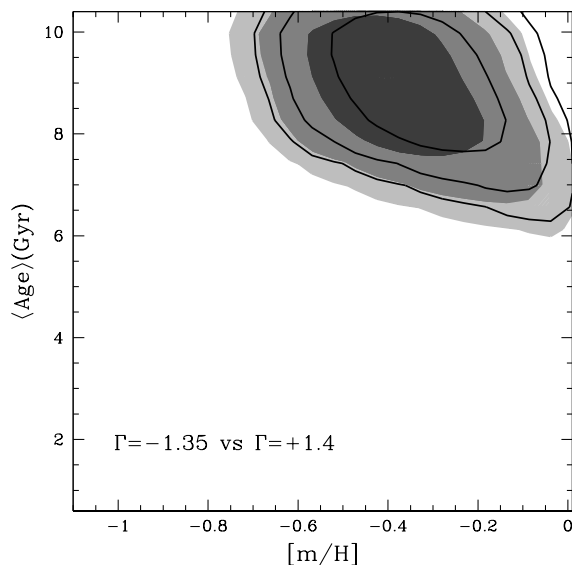


**Figure 3.** The 68, 95 and 99% confidence levels in metallicity and average age are shown for the  $\tau$  models described in the text, using the Pégasé-HR (High Resolution) library. The greyscale corresponds to an IMF with slope  $\Gamma = +1.35$  (i.e. Salpeter), whereas the lines represent the other extreme explored in this paper ( $\Gamma = -1.4$ ).

Our reference image is taken from the CASTLES survey<sup>1</sup>. It is a 384 second exposure with NIC2/HST through passband F160W. The lensing analysis only uses the redshifts of the QSO and of the lens, along with the QSO image positions to constrain the surface mass density on the lens plane. The NICMOS image is also used to reconstruct the surface brightness profile of the lens. We use GALFIT (Peng et al. 2002) in order to remove the unresolved images of the background QSO (see Leier et al. 2010, for details). Figure 1 shows the cumulative mass and H-band luminosity profiles of the lens. The uncertainties in lensing mass and luminosity are given by the shaded region and errorbars, respectively. Notice the lens geometry allows us to constrain in detail the cumulative mass within  $R \lesssim 0.75$  kpc, roughly around one effective radius (top axis).

The range of lens models has a characteristic butterfly shape, which can be understood as follows. For a pure Einstein ring, the enclosed mass  $M(< R)$  is perfectly constrained at the Einstein ring, but degenerate at any other radius. Now, the prior allows mass profiles ranging from  $R^{-1/2}$  to a point mass, hence  $M(< R)$  can range from  $R^{3/2}$  to flat. The maximal and minimal values of steepness, combined with the Einstein-radius constraint, shape the allowed range of models. In practice, because real lenses are not pure Einstein rings, the range of models is not quite so extreme, but retains the butterfly shape. The inset shows the H-band frame of the lens and quasar images along with their standard identifications. The mass and luminosity profiles are compared to obtain the H-band mass-to-light ratio ( $\Upsilon_H$ ), as shown in figure 2, including the uncertainty as a shaded region. The point where the errorbar is smallest is chosen to constrain the low-mass end of the IMF. The figure shows that within this region, the lensing galaxy has an average  $\Upsilon_H = 1.19 \pm 0.16$  (90% confidence level).

Our next step involves the construction of a large number of composite stellar populations, following an exponentially decay-

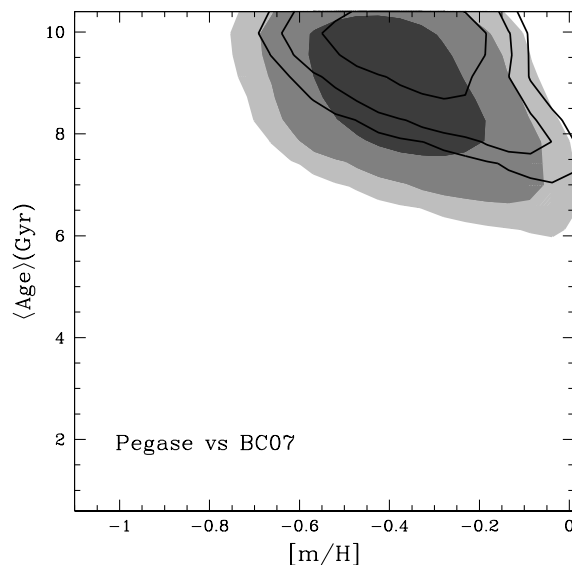


**Figure 4.** Same as figure 3 comparing two different sets of models, both assuming a Salpeter IMF. The greyscale corresponds to Pégasé-HR, and the lines are the predictions of the BC07 models (see text for details).

ing star formation history. Hence, each model is characterised by the formation epoch, decay timescale and metallicity. We also need to consider different sets of models for a number of choices of the IMF. Notice these are composite models and not simple stellar populations (SSPs), therefore giving more robust mass-weighted values. SSP-determined values are easily affected by the presence of recent star formation, even with small amounts of young stars, resulting in – sometimes significantly – lower M/L ratios (see e.g. Rogers et al. 2010).

In previous work (Ferreras et al. 2005, 2008; Leier et al. 2010) we used broadband photometry to constrain the mass-to-light ratio of the stellar populations. We showed that acceptable uncertainties can be obtained on M/L even though one should not use broadband photometry alone to constrain the age and metallicity of the unresolved populations (see e.g. Gallazzi & Bell 2009). However, in order to minimise the uncertainties in the estimates of M/L, we use deep spectroscopic observations of the Einstein Cross from VLT/FORS1 with grism G300V, giving a spectral resolution of  $R \sim 400$  at  $5900\text{\AA}$  (Eigenbrod et al. 2008). The spectra are taken at two slit positions: mask 1 ( $t_{\text{EXP}}=11.70\text{h}$ ) at  $\text{PA} = -56.5^\circ$ , passing through images A and D; and mask 2 ( $t_{\text{EXP}}=11.25\text{h}$ ) at  $\text{PA} = -68.5^\circ$ , passing through images B and C (see figure 1). The 2D spectra are separated into a point source – the quasar spectrum – and an extended source – the lens. The method leaves no trace of the emission line spectrum of the quasar in the lens spectrum, which can be seen in figure 7 of Eigenbrod et al. (2008).

We measure the equivalent widths (EWs) of a number of age and metallicity sensitive spectral features: Balmer  $H\beta$ ,  $H\gamma$ ,  $H\delta$ , Mgb, Fe5270, Fe5335, G4300 and the  $4000\text{\AA}$  break. The EWs are determined using a recent definition of the continuum (Rogers et al. 2010) that reduces the contamination in EW estimates from neighbouring lines, improving on the discrimination between age and metallicity.

We also have at our disposal the HST/NICMOS (F160W) and HST/WFPC2 (F555W and F814W) images. Note we already use the F160W image to determine the maximum  $\Upsilon_H$  from stars. How-

<sup>1</sup> <http://www.cfa.harvard.edu/castles>

ever, we can combine these three bands to generate two colours. At the effective radius, the colours are  $V - I = 1.28$  and  $I - H = 1.89$  (Using Vega as zero-colour reference). The  $1\sigma$  photometric uncertainties stay around 0.05 mag in both colours. The colour gradient is very shallow: over the  $R < 2R_e$  range, the gradients  $\Delta\text{Colour}/\Delta(R/R_e)$  are  $-0.003$  and  $0.05$  in  $V - I$  and  $I - H$ , respectively. The flat colour profile confirms the homogeneity of the stellar populations in this lens. The colours help further constrain the stellar populations, although we emphasize that the inclusion of the colours does not improve significantly the estimates based on EWs, as expected.

From the available stellar population synthesis models, we chose the high spectral resolution version of Pégasé (Le Borgne et al. 2004). These models allow the user to recalculate the spectra of simple stellar populations for an arbitrary choice of IMF. Our goal is to constrain the shape of the low-mass end of the IMF. Hence, we decided to model the IMF as two power laws, defined as follows:

$$\frac{dN}{d\log M} \propto \begin{cases} M^{-\Gamma} & 0.1 < M/M_\odot < 1 \\ M^{-1.35} & 1 < M/M_\odot < 100 \end{cases} \quad (1)$$

The above definition follows Kroupa (2007), although we select the Salpeter IMF slope (Salpeter 1955) at the high mass end and choose  $1M_\odot$  for the position of the knee. For masses below this knee, we parameterise the IMF as a power law with index  $\Gamma$ . We explore a wide range of values, from  $\Gamma = -1.4$  to  $+1.4$  (where a Salpeter IMF corresponds to  $\Gamma = +1.35$ ). For each choice of  $\Gamma$ , we generate a set of base models (simple populations) that are combined into composite  $\tau$ -models as described above, covering a grid of  $48 \times 48 \times 48$  models over a range of formation epoch ( $2 \leq z_{\text{FOR}} \leq 10$ ); decay timescale ( $-1 \leq \log(\tau/1\text{Gyr}) \leq +1$ ) and metallicity ( $-1 \leq [m/H] \leq +0.3$ ). Hence, our methodology takes into account a spread in the age distribution, an important issue when dealing with the stellar populations of galaxies (see e.g. Rogers et al. 2010). Each choice of star formation history gives a set of EWs and colours that are compared with the observations via a standard  $\chi^2$ -defined likelihood to infer the probability distribution function. The synthetic spectra are broadened to the spectral resolution of the observations, taking also into account the observed velocity dispersion of the lens,  $\sigma = 166 \pm 2$  km/s (van de Ven et al. 2008). Also notice that the constraint on the M/L ratio shown in figure 2 corresponds to the *observed frame* H-band. The models take into account the minor K-correction needed, given the redshift of the lens.

### 3 THE SYSTEMATICS OF STELLAR MAS ESTIMATES

It is important to understand the systematic effects caused by the choice of population synthesis models in the estimates of stellar mass. Firstly, we consider the effect that a different choice of slope would have on the predicted average age and metallicity of the lens galaxy. Figure 3 shows the probability distribution of the average age and metallicity between the two extreme choices of IMF: namely a Salpeter IMF ( $\Gamma = +1.35$ , greyscale) and a strong suppression of low-mass stars ( $\Gamma = -1.4$ , lines). One can see that within error bars, the average age and metallicity are unchanged, corresponding to an old ( $\gtrsim 8$  Gyr) population.

Different population synthesis models rely on their choices of stellar evolution prescriptions, isochrones, and stellar libraries. We quantify this effect in the following two figures. Figure 4 shows

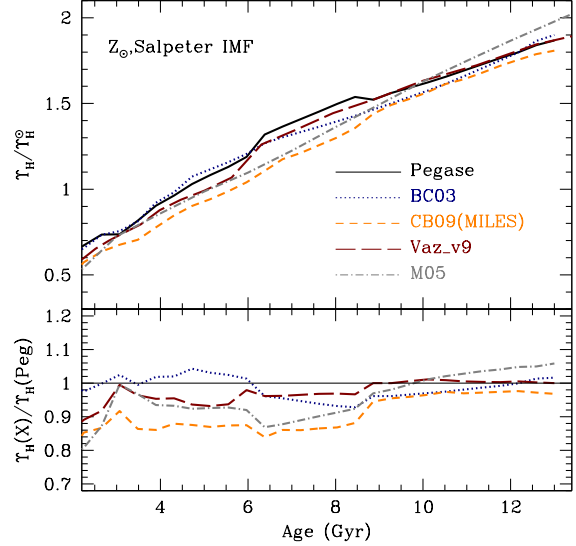


**Figure 5.** Comparison of the H-band stellar mass-to-light ratio predicted by a number of population synthesis models. For ease of comparison, we consider here only simple stellar populations with solar metallicity and a Salpeter IMF. The models are Pégasé (black solid line, Le Borgne et al. 2004); two different flavours of the GALAXEV models: BC03 (blue dotted line Bruzual & Charlot 2003); and the recent, unpublished 2009 models including the MILES spectral library (orange short dashed lines, private communication, and Sánchez-Blázquez et al. 2006); Vazdekis/MILES models v.9 (long dashed lines Vazdekis et al. 2010) and Maraston (grey dot-dashed lines, 2005). The bottom panel shows the ratio with respect to the fiducial Pégasé-HR models used in this paper.

the age and metallicity probability distribution for a Salpeter IMF using two independent models: Pégasé (grayscale) and Bruzual & Charlot (2003; lines). The latter tends to give slightly older ages, although the confidence levels overlap, eliminating the chance of a systematic offset caused by a different age or metallicity.

To emphasize this point, figure 5 illustrates the predictions in  $\Upsilon_H$  for a range of Simple Stellar Populations of solar metallicity – as suggested by the best fits shown in the previous figures. Various population synthesis models are shown, as labelled. Hence, for the age range considered to be a best fit ( $\gtrsim 8$  Gyr), the systematic difference between these models cannot be larger than  $\sim 10\%$ . Another possible systematic source would be the presence of dust, mainly in the disc of the lens galaxy. Eigenbrod et al. (2008) showed that the  $V$ -band differential extinction caused by the lens on the background quasar is in the range 0.1–0.3 mag. Using a standard extinction law (e.g. Fitzpatrick 1999), we estimate an attenuation no larger than about 0.05 mag in the H band. Hence, the net systematic uncertainty on the determination of the stellar masses is  $\sim 15 - 20\%$ .

### 4 RESULTS

Figure 6 shows the constraint on the stellar  $\Upsilon_H$  from the photo-spectroscopic data, as a function of IMF low-mass slope. For reference, the upper limit to the  $\Upsilon_H$  from lensing is shown as a horizontal line along with the 90% confidence level (dashed lines). A Salpeter IMF ( $\Gamma = +1.35$ ) clearly gives a stellar  $\Upsilon_H$  that is too high with respect to the lensing estimate. The best fits are shown

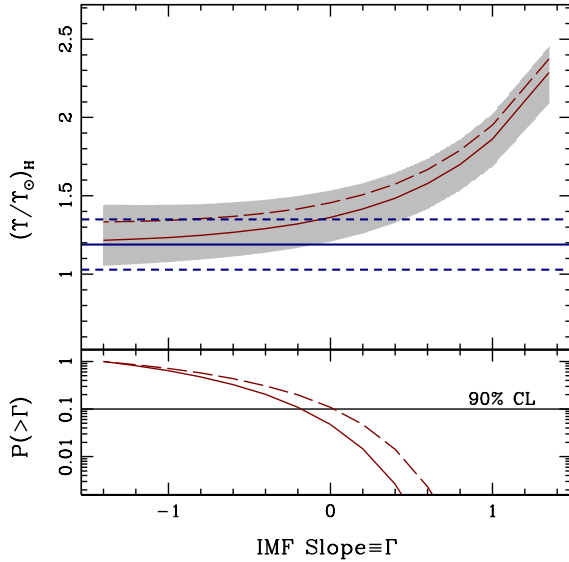


**Figure 6.** *Top:* Constraints at the 90% confidence level from the observed equivalent widths of Balmer lines ( $H\beta$ ,  $H\gamma$ ,  $H\delta$ ); the metal sensitive  $[\text{MgFe}]$  index; and the  $V - I$  and  $I - H$  colours. The result is shown as a function of the low-mass slope of the IMF. The shaded region corresponds to the  $\Upsilon_H$  given by the Pégasé-HR models used in this paper. The horizontal lines give the 90% confidence level for the predicted M/L using lensing data and the observed photometric profile of the lens (see figure 2). The solid (long dashed) curved lines correspond to slit 1 and 2, respectively, with the shaded region extending over the 90% confidence level for both slits 1 and 2. *Bottom:* Cumulative joint probability of the IMF slope, given the lensing estimate of  $\Upsilon_H$  and the population synthesis constraints. A Salpeter IMF ( $\Gamma = +1.35$  is ruled out at more than the 99% confidence level. At a 90% level, slopes  $\Gamma > 0$  are rejected as well.

as curved solid and long-dashed lines for the analysis of spectra from masks 1 and 2, respectively. The result is compatible within the 90% confidence level (grey shaded area). Furthermore, our data can constrain in more detail the low-mass end of the IMF. The lower panel of figure 6 shows the cumulative probability distribution function,  $P(> \Gamma)$ . At a 90% confidence level, slopes  $\Gamma > 0$  are ruled out.

Our modelling has taken an “integrated approach” to the presence of disk and bulge. Indeed, both the spectroscopic and the photometric data have not been separated into a bulge and a disk component. Hence, the modelling of the data corresponds to an “average” stellar population which would be dominated by the old component, given that most of the light originates from the central region of the galaxy, a point confirmed by the old ages and high metallicities predicted by the modelling (see figures 3 and 4). The photometric analysis is done in a non-parametric way, hence we compute stellar masses from this “composite population” of disk and bulge stars in a consistent way. Were we to remove the presence of the disk population, the older bulge stars would result into higher  $\Upsilon_H$  therefore making a Salpeter IMF even more incompatible with the observations. Finally, a significant presence of dark matter in the inner regions of galaxies (see e.g. Tortora et al. 2009) will make the rejected models even more unlikely, since the analysis presented here predicts more stellar mass than lensing mass for those rejected models. Therefore, our conclusions are robust with respect to the complex populations of disk and bulge stars, or to the presence of dark matter.

## ACKNOWLEDGMENTS

FC is partially supported by the SNSF (Switzerland).

## REFERENCES

- Bruzual, G., Charlot, S., 2003, *MNRAS*, 344, 1000  
 Bruzual, G. 2007, IAU No. 241 Symp. Procs. “Stellar populations as building blocks of galaxies”, eds. A. Vazdekis and R. F. Peletier, Cambridge, arXiv:astro-ph/0703052  
 Andersen, M., Meyer, M. R., Greissl, J., Aversa, A., 2008, *ApJ*, 683, L183  
 Auger, M. W., Treu, T., Gavazzi, R., Bolton, A. S., Koopmans, L. V. E. & Marshall, P. J. 2010, arXiv:1007.2409  
 Bastian, N., Covey, K. R., Meyer, M. R., 2010, *ARA&A*, in press, arXiv:1001.2965  
 Cappellari, M., et al. 2006, *MNRAS*, 366, 1126  
 Chabrier, G., 2003, *PASP*, 115, 763  
 Coccato, L., et al. 2009, *MNRAS*, 394, 1249  
 Coles, J., 2008, *ApJ*, 679, 17  
 Eigenbrod, A., Courbin, F., Sluse, D., Meylan, G., Agol, E., 2008, *A&A*, 480, 647  
 Falco, E. E., Gorenstein, M. V. & Shapiro, I. I., 1985, *ApJ*, 289, L1  
 Ferreras, I., Saha, P., Williams, L. L. R., 2005, *ApJ*, 623, L5  
 Ferreras, I., Saha, P., Burles, S., 2008, *MNRAS*, 383, 857  
 Fitzpatrick, E. L., 1999, *PASP*, 111, 63  
 Gallazzi, A., Bell, E. F., 2009, *ApJS*, 185, 253  
 Huchra, J., Gorenstein, M., Kent, S., Shapiro, I., Smith, G., Horne, E., Perley, R., 1985, *AJ*, 90, 691  
 Kroupa, P., 2007, arXiv:astro-ph/0703282  
 Kroupa, P., 2002, *Science*, 295, 82  
 Larson, R. B., 1998, *MNRAS*, 301, 569  
 Larson, R. B., 2006, *Rev. Mex. AA*, 26, 55  
 Leier, D., Ferreras, I., Saha, P., Falco, E. E., 2010, *MNRAS*, submitted.  
 Le Borgne, D., Rocca-Volmerange, B., Prugniel, P., Lançon, A., Fioc, M., Soubiran, C., 2004, *A&A*, 425, 881  
 Liesenborgs, J., De Rijcke, S., Dejonghe, H. & Bekaert, P., 2008, *MNRAS*, 386, 307  
 Maraston, C., 2005, *MNRAS*, 362, 799  
 Peng, C. Y., Ho, L. C., Impey, C. D., Rix, H., 2002, *AJ*, 124, 266  
 Rogers, B., Ferreras, I., Peletier, R. F., Silk, J., 2010, *MNRAS*, 402, 447  
 Rusin, D. et al. 2003, *ApJ*, 587, 143  
 Saha, P., 2000, *AJ*, 120, 1654  
 Saha, P., Williams, L. L. R., 2004, *AJ*, 127, 2604  
 Saha, P., Williams, L. L. R., 2006, *ApJ*, 653, 936  
 Salpeter, E. E., 1955, *ApJ*, 121, 161  
 Sánchez-Blázquez, P., et al., 2006, *MNRAS*, 371, 703  
 Tortora, C., Napolitano, N. R., Romanowsky, A. J., Capaccioli, M., Covone, G., 2009, *MNRAS*, 396, 1132  
 Treu, T., Auger, M. W., Koopmans, L. V., Gavazzi, R., Marshall, P. J. & Bolton, A. S. 2010, *ApJ*, 709, 1195  
 Trott, C. M., Treu, T., Koopmans, L. V. E., Webster, R. L., 2010, *MNRAS*, 401, 1540  
 van de Ven, G., Falcón-Barroso, J., McDermid, R. M., Cappellari, M., Miller, B. W., de Zeeuw, P. T., 2008, arXiv:0807.4175  
 Vazdekis, A., Sánchez-Blázquez, P., Falcón-Barroso, J., Cenarro, A. J., Beasley, M. A., Cardiel, N., Gorgas, J., Peletier, R. F., 2010, *MNRAS*, in press, arXiv:1004.4439